CEAS EuroGNC 2019
"Conference on Guidance, Navigation and Control"
3-5 April 2019 @ Politecnico di Milano, Milan, Italy.

CEAS-GNC-2019-021

POLITECNICO
MILANO 1863

A Generic Rendezvous Control Solution for Automatic Landing of Unmanned Aircraft

Julian Theis and Frank Thielecke

Abstract A generic model of a track-based landing system is formulated and a complete controller layout for motion synchronization with an approaching aircraft is proposed. All required control system parameters are derived in closed form from basic loopshaping principles. They establish a generic solution parameterized in dependence on only a small number of model parameters. That is, there is no need to tune controllers. This way of selecting the parameters further provides significant insight into achievable performance. This insight can then be used to derive requirements for particular realizations on the system level. Exemplary simulation studies with a representative aircraft model and autopilot algorithms demonstrate the high-precision of the proposed controller. Further, robustness with respect to parameter uncertainty is concluded from Monte-Carlo evaluation.

1 Introduction

Automated landing of unmanned aircraft is a high precision control task. This is particularly true for high altitude long endurance (HALE) and pseudo-satellite (HAPS) aircraft. HALE/HAPS aircraft stay airborne for several days, weeks or even months and will possibly provide a low-cost alternative to satellite systems for surveillance, reconnaissance, relay purposes, and remote sensing. Extreme aerodynamic efficiency and low weight are crucial for achieving such long endurance. Further, take-off and landing are only very small parts of the mission profile. Omitting a landing gear on the UAV therefore appears to be a promising strategy to increase performance. Doing so, however, necessitates a ground-based landing system capable of reliably replacing the landing gear's functionality. Such ground-based systems are envisioned, e. g., in [2, 13, 16, 21, 24]. In this paper, track-based systems are con-

Julian Theis · Frank Thielecke
Institute of Aircraft Systems Engineering, Hamburg University of Technology, Nesspriel 5, 21129 Hamburg, Germany, e-mail: julian.theis@tuhh.de, e-mail: frank.thielecke@tuhh.de

sidered. They consist of a track on which a trolley is moving such that it establishes position and velocity synchronization with an approaching aircraft, [2, 16, 24]. An additional benefit of such a system is its ability to offset yaw angle when an aircraft approaches crabbed, [17]. A crabbed approach is usually performed in crosswind conditions and necessitates a decrab maneuver before touchdown, which can be challenging.

The paper starts with a detailed description of the rendezvous control problem for automatic landing in Section 2. A generic model of a track-based landing system is formulated and a complete controller layout is proposed in Section 3. All control system parameters are derived from basic loopshaping principles. They establish a generic solution parameterized in dependence on the model parameters. It is further shown that this way of selecting the parameters provides significant insight into achievable performance. The simulation environment for evaluation of the proposed controller is described in Section 4. Finally, exemplary simulation studies with a representative aircraft model and autopilot algorithms are performed in Section 5. These studies also consider large parameter uncertainties to demonstrate the inherent robustness of the proposed control solution.

2 Problem Statement

Automated landing of an unmanned aircraft on a track-based landing system requires advanced control systems for both participants. Let $[x_{\text{aircraft}}\ y_{\text{aircraft}}\ z_{\text{aircraft}}]$ denote the aircraft's position in a local reference frame with z pointing towards the center of earth, x pointing in the direction of the ground system track, and y completing a Cartesian system. Let further $[x\ y\ z]$ denote the position of the landing system's dedicated contact point in the same coordinate frame.

The aircraft and the landing system must synchronize their position to perform a successful landing, i. e., $x(t) = x_{\text{aircraft}}(t)$ and $y(t) = y_{\text{aircraft}}(t)$ for t: $z(t) = z_{\text{aircraft}}(t)$. In order to minimize impact forces, it is further desirable to also synchronize the velocities, i. e., $\dot{x}(t) = \dot{x}_{\text{aircraft}}(t)$ and $\dot{y}(t) = \dot{y}_{\text{aircraft}}(t)$ for t: $z(t) = z_{\text{aircraft}}(t)$. The aircraft's velocity, expressed in the local reference frame is

$$\begin{bmatrix} \dot{x}_{\text{aircraft}} \\ \dot{y}_{\text{aircraft}} \\ \dot{z}_{\text{aircraft}} \end{bmatrix} = \begin{bmatrix} \cos(\chi - \chi_{\text{ref}}) & 0 \\ \sin(\chi - \chi_{\text{ref}}) & 0 \\ 0 & 1 \end{bmatrix} \begin{bmatrix} V_{\text{ground}} \\ V_{\text{vertical}} \end{bmatrix} \tag{1}$$

where χ denotes the course angle measured from north about the z-axis and χ_{ref} is the heading angle of the ground system track. The ground speed V_{ground} is the speed of the aircraft relative to earth in the xy-plane and V_{vertical} is the speed in z-direction, i. e., the sink rate. Equation (1) highlights the well-known fact that the aircraft position is subject to non-holonomic constraints in a Cartesian coordinate system. Among other factors, this makes precise control of the aircraft velocity and position significantly more difficult than controlling the position and velocity of a

fully-actuated landing system. Such a fully actuated kinematic configuration is proposed in [2], where the landing system consists of a trolley which moves along tracks. On top of this trolley, a second trolley is mounted to account for lateral displacement. A third moving part, the contact rack, is mounted on the second trolley and adjusts for the yaw angle.

Hence, the aircraft is considered to simply follow a predefined approach path along the centerline of the landing system, resembling current standard landing procedures for commercial aircraft. The approaching aircraft must, however, stay in close proximity to the centerline as the lateral extend of the landing system is limited. The ground system must then synchronize its motion with the aircraft and compensate deviations of the aircraft from its ideal flight path. Ideally, the trolley should stay in front of the aircraft at all times to avoid collisions. That means, a small velocity offset is desirable such that the trolley is slightly slower than the aircraft. The aircraft closes the gap with low relative velocity and overshoot is avoided. On the other hand, synchronization must happen as fast as possible since the length of the track is limited.

3 Ground System Modeling and Control

A rigid multi-body model is proposed based on a simple Newtonian formulation of the three independent degrees of freedom (x along the track, y perpendicular to the track, Ψ angular adjustment; see Figure 1).
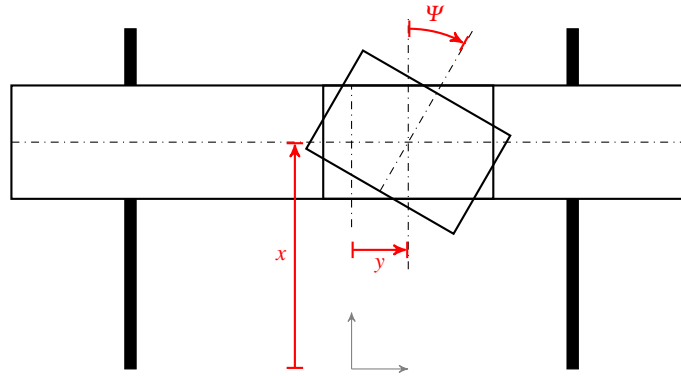
Fig. 1 Multi-body system representing a track-based landing system with three generalized coordinates.

The dynamics of the two trolleys are modeled as point masses subject to controlled forces. The rotary dynamics of the contact rack is modeled as a point inertia subject to a controlled moment. Damping coefficients lump together effects such as rolling friction and air resistance. The equations of motions in the generalized

coordinates x, y, Ψ are

$$m_x \ddot{x} + d_x \dot{x} = F_x \tag{2a}$$

$$m_y \ddot{y} + d_y \dot{y} = F_y \tag{2b}$$

$$J_\Psi \ddot{\Psi} + d_\Psi \dot{\Psi} = M_\Psi, \tag{2c}$$

where m_x, m_y, and J_Ψ denote the generalized masses, d_x, d_y, d_Ψ denote damping coefficients, and F_x, F_y, M_Ψ denote the generalized forces associated with each degree of freedom. The model (2) captures the relevant dynamics despite its apparent simplicity. Owing to this simplicity, it is possible to derive explicit solutions for the rendezvous control problem in the following sections.
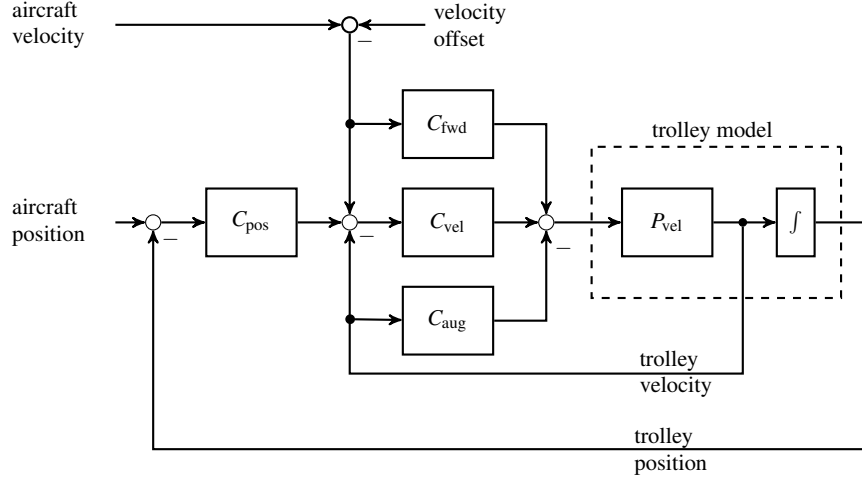
3.1 Control Systems Architecture

The decoupled three-axes-motion of the landing system with second-order dynamics in each of the three degrees of freedom lends itself very naturally to a velocity-position cascade control structure (cf., e. g. [1, 15]). The cascade structure exploits the physical integration step from velocity to position: In case the trolley has the correct velocity, but a wrong position, the position error causes a velocity demand which reduces the error. When the position is synchronized, the trolley follows the aircraft's velocity, i. e., also maintains velocity synchronization. Such a structure was also used in [17, 24] for controlling a landing system and proved to be suitable.

In this paper, an extended controller layout, depicted in Figure 2 is proposed. The inner control loop tracks the aircraft velocity, adjusted for a predefined offset. A two-degrees-of-freedom control architecture is used to meet the high dynamic response requirement for a successful rendezvous maneuver. To this end, C_{vel} is designed as a proportional-integral compensator which processes the velocity error, while C_{aug} is a proportional compensator which feeds back the measured velocity. This setup can avoid the slow response that is usually associated with the slow damping pole of the model. To further ease the choice of design parameters, an explicit feedforward compensator C_{fwd} is added. The position control loop provides a velocity correction signal, calculated by a proportional controller C_{pos}, such that the aircraft position is tracked. This controller layout is applied to all three degrees of freedom. That is, it is used to control position and velocity along the track $(x, \dot{x})$, position and velocity perpendicular to the track $(y, \dot{y})$, and the yaw angle and rate $(\Psi, \dot{\Psi})$.

Each of the control loops can be designed following classical loopshaping guidelines. Loopshaping is a classical design technique for single-input-single-output systems (e. g. [7, 10]). It is based on "shaping" the looptransfer $L = PC$ such that it resembles $L_{\text{ideal}} = \frac{\omega}{s}$. Hence, the ideal compensator is $C_{\text{ideal}} = \frac{\omega}{s} P^{-1}$. It inverts the plant dynamics and adds integral action. Such a complete inversion is often neither possible nor desirable for reasons of control effort and robustness. Thus, the standard strategy is to select a compensator such the $\frac{\omega}{s}$-loopshape is approximately attained around the desired crossover frequency with sufficient gain in the low-frequency

regime. The simple model structure of the problem at hand, however, makes it possible to derive a generic solution to the problem in terms of the model parameters. This solution also provides additional insight into the fundamental limitations of the control problem.

Fig. 2 Control architecture for synchronization of aircraft and trolley.

3.2 Generic Control System Parameters

The transfer function from each of the generalized forces to the corresponding generalized velocity is of the form

$$P_{\text{vel}}(s) = \frac{\frac{1}{m}}{\left(s + \frac{d}{m}\right)(s\tau + 1)}, \tag{3}$$

where first order actuator dynamics with a time constant τ are included. That is, the transfer function has poles at $s = -1/\tau$ and $s = -d/m$. For any well-posed problem, the actuator dynamics are much faster than the damping dynamics and hence $d/m \ll 1/\tau$.

First, the feedforward compensator C_{fwd} can be selected such that it inverts P_{vel} in steady state. That is,

$$C_{\text{fwd}} = P_{\text{vel}}^{-1}(0) = d. \tag{4}$$

With this choice, the feedforward compensator demands exactly the force that the ground system requires to maintain the aircraft's velocity. The inevitable inaccuracy of the damping parameter, however, still necessitates the use of integral control

on the velocity error, established through C_{vel}. The slow damping dynamics motivate augmentation of the system dynamics by means of the compensator C_{aug} prior to designing the velocity control loop. Without this compensator (i. e. with a single-degree-of-freedom controller), the standard design would involve cancellation of the slow pole by the controller zero. Unfortunately, this would result in a slow and sluggish response. Therefore, the first design step is to close the augmentation feedback loop. Doing so yields the transfer function

$$P_{\text{vel,aug}}(s) = \frac{P_{\text{vel}}(s)}{1 + P_{\text{vel}}(s)\,C_{\text{aug}}} = \frac{\frac{1}{\tau m}}{s^2 + s\left(\frac{1}{\tau} + \frac{d}{m}\right) + \frac{d + C_{\text{aug}}}{\tau m}}. \tag{5}$$

Both the damping ratio ζ_{aug} and natural frequency ω_a of the augmented system are affected by this loop closure. The gain C_{aug} is now selected such that a desired damping ratio is achieved, yielding

$$C_{\text{aug}} = \tau m \left(\frac{\frac{1}{\tau} + \frac{d}{m}}{2\,\zeta_{\text{aug}}} \right)^2 - d. \tag{6}$$

With this choice, the augmented system (5) becomes

$$P_{\text{vel,aug}}(s) = \frac{\frac{1}{\tau m}}{s^2 + 2\,\zeta_{\text{aug}}\,\omega_a\,s + \omega_a^2} \quad \text{with} \quad \omega_a = \frac{\frac{1}{\tau} + \frac{d}{m}}{2\,\zeta_{\text{aug}}}. \tag{7}$$

In order to permit a complete analytical solution, ζ_{aug} is fixed to $\zeta_{\text{aug}} = 0.7$. This damping ratio corresponds to a response characteristic that is usually considered desirable: fast response with very little overshoot (cf., e. g. [20]). Further, a phase margin of $70°$ can be inferred, which is a reasonable value, given the low-fidelity of the design model.

Using the parameterization

$$C_{\text{vel}}(s) = k_P \frac{s + k_I}{s} \tag{8}$$

and the selected value $\zeta_{\text{aug}} = 0.7$, the loop transfer for velocity control of the augmented system becomes

$$L_{\text{vel}}(s) = P_{\text{vel,aug}}(s)\,C_{\text{vel}}(s) = \frac{\frac{k_P}{\tau m}\,(s + k_I)}{s(s^2 + 1.4\,\omega_a\,s + \omega_a^2)}. \tag{9}$$

Following the loopshaping paradigm, the controller zero is placed at the corner frequency of the augmented system, leading to

$$k_I = \omega_a = \frac{\frac{1}{\tau} + \frac{d}{m}}{1.4}. \tag{10}$$

The final step is to select the crossover frequency and hence k_P. The particular pole-zero pattern of the loop transfer (9) with the $k_I = \omega_a$ justifies the approximation

$$|L_{\text{vel}}(j\omega)| \approx \frac{k_P}{\omega_a \tau m} \left| \frac{1}{j\omega} \right| \quad \text{for} \quad \omega < \omega_a. \tag{11}$$

Consequently, the proportional gain k_P that establishes a desired crossover frequency $\omega_b < \omega_a$ is obtained as

$$k_P = \tau m \omega_a \omega_b. \tag{12}$$

A reasonable approach to select ω_b is to maximize the crossover frequency under a phase margin constraint. With $k_I = \omega_a$, the phase of the loop transfer (9) in dependence on ω_a can be calculated analytically. When a phase margin constraint of $70°$ is considered, the maximum frequency is $\omega_b = 0.57\,\omega_a$. Using this choice, Equation (12) becomes

$$k_P = 0.57\,\tau m \left(\frac{\frac{1}{\tau} + \frac{d}{m}}{1.4} \right)^2. \tag{13}$$

Similarly, a controller gain for the position cascade can be derived using

$$L_{\text{pos}}(s) = \frac{1}{s} \frac{L_{\text{vel}}(s)}{1 + L_{\text{vel}}(s)} C_{\text{pos}}. \tag{14}$$

When a $60°$ phase margin is considered sufficient for the outer control loop, a desired crossover frequency $\omega_c = 0.3\,\omega_b$ is obtained. Consequently, the controller gain is

$$C_{\text{pos}} = 0.3\,\omega_b = 0.171 \frac{\frac{1}{\tau} + \frac{d}{m}}{1.4}. \tag{15}$$

The position control loop bandwidth ω_c also indicates the speed of response of the overall synchronization process. Hence, it directly yields an estimate of achievable performance for the rendezvous controller, based solely on three simple model parameters.

3.3 Activation and Switching Logic

The trolley should synchronize its motion as fast as possible with the aircraft. Therefore, an activation distance is calculated from the current aircraft ground speed and the maximum trolley acceleration $a_{\text{max}} = F_{x,\text{max}}/m_x$. Once the aircraft reaches the activation distance $x_{\text{activation}}$, the x-velocity control loop, the y-position control loop, and the yaw angle control loop are activated. As a consequence, the landing system starts to accelerate along the track. The trolley mounted perpendicular to the track direction acquires the aircraft's lateral position and velocity and the contact rack is aligned with the aircraft heading angle. When a specified switching distance

$x_{\text{switch,pos}}$ is reached, the longitudinal position control loop is activated and the velocity offset term V_{offset} is set to zero. That is, the velocity reference signal is now adjusted such that *both* velocity and position synchronization are achieved.

To ensure that synchronization is achieved as fast as possible, the activation distance is calculated in dependence on the aircraft's approach velocity. A constant approach velocity V_{aircraft} is assumed and actuator dynamics are neglected for this calculation. Thus, the trolley acceleration after activation is assumed to be identical to a_{max} until the target velocity $V_{\text{aircraft}} - V_{\text{offset}}$ is reached. The required time for velocity synchronization under this assumption is $t_{\text{sync}} = (V_{\text{aircraft}} - V_{\text{offset}})/a_{\text{max}}$ and the aircraft position is

$$x_{\text{aircraft}}(t_{\text{sync}}) = V_{\text{aircraft}} \frac{V_{\text{aircraft}} - V_{\text{offset}}}{a_{\text{max}}} - x_{\text{activate}}. \tag{16}$$

The trolley position at this instant in time is

$$x_{\text{trolley}}(t_{\text{sync}}) = \frac{1}{2} \frac{(V_{\text{aircraft}} - V_{\text{offset}})^2}{a_{\text{max}}}. \tag{17}$$

Equating the positions and adding a desired relative distance x_{offset}, the optimal activation distance is calculated as

$$x_{\text{activate}} = V_{\text{aircraft}} \frac{(V_{\text{aircraft}} - V_{\text{offset}})}{a_{\text{max}}} - \frac{1}{2} \frac{(V_{\text{aircraft}} - V_{\text{offset}})^2}{a_{\text{max}}} + x_{\text{offset}}. \tag{18}$$

### 3.4 Measurements and Signal Processing

It is assumed that the position and velocity of the ground system trolleys can be measured with sufficient accuracy. Further, onboard measurements of aircraft's ground speed, attitude, and GPS-position are assumed to be available such that a transformation into the local reference frame of the ground system is possible. These measurements provide the references for the control system, i. e. they are not part of a feedback loop from the perspective of the landing system. Nevertheless, accuracy of the rendezvous maneuver critically depends on accurate information about the current aircraft position and velocity. Commercial-of-the-shelf low-cost equipment currently provides GPS data with a sampling rate of 1-10 Hz. Further, a downlink from the aircraft to the ground system needs to be established which introduces additional delay. Even if the unrealistic assumption of perfect accuracy and latency-free transmission is made, such a low sample rates poses a severe challenge for the rendezvous maneuver. A 10 Hz sampling rate, e. g., means that a position signal is available only every meter for an aircraft approaching with a speed of 10 m/s. Achieving an accuracy on the scale of centimeters is hence far from trivial.

In order to address the problem of low sampling rates, Kalman filters are used to augment the data transmitted by the aircraft. The velocities in the local coordinate

system are used as inputs to integrator models which predict the position between measurements. Once a new position measurement is available, it is used to update the prediction through a feedback gain. That is, the Kalman filter performs a sensor fusion of velocity and position signal, much in the fashion of a complementary filter, to "upsample" the position signal. Figure 3 shows an example of such an upsampled signal. This signal is clearly better suited for control purposes, but still exhibits the time delay of the transmission. If this delay is known, e. g., from comparing the GPS time-stamps of the transmitted signals and a local GPS receiver, this effect can also be compensated.

Fig. 3 Kalman filter prediction (——) of the actual aircraft position ($\cdots\cdots$) using the transmitted low-sample rate information (——).
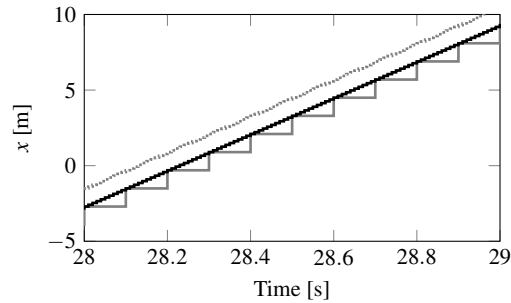
4 Simulation Environment

An in-house developed generic flight simulation environment is used to evaluate the proposed ground controller in conjunction with the model of a landing aircraft. This environment, called *FLYSIM*, provides a modular Matlab/Simulink component library [12]. It implements a standard nonlinear six-degrees-of-freedom rigid-body flight mechanics model (see, e. g., [3, 4, 14] for details) in order to simulate the approaching aircraft. The *FLYSIM* simulation environment also contains models for stall and ground effect as described in [11]. An earth geoid model according to the WGS84 standard [5] with international standard atmosphere completes the environment. It is further possible to simulate gusts and wind shear in accordance with MIL-STD-1797 [6] and EASA CS-25 [8].

4.1 Aircraft Model and Autopilot

For the simulation studies, a model of the aircraft depicted in Figure 4 is considered. The aircraft is a low-cost test platform with a large aspect ratio of 26. It was built in-house as a first step towards experimental investigation of HAPS-like aircraft. The aircraft has a mass of approximately 4 kg and a wing span of 4.5 m. Aerodynamic coefficients were estimated from flight test data using standard parameter identification methods [11].

Fig. 4 Large aspect-ratio low-cost test aircraft *TriHeron*.
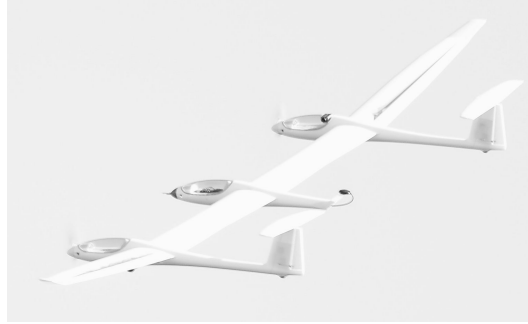
The architecture for the longitudinal autopilot of the considered aircraft is depicted in Figure 5. It uses the elevator δ_e to control the vertical speed as the primary longitudinal control variable, similar to, e. g., [19]. In conjunction with an autothrottle that controls forward velocity through thrust δ_{th}, this approach is essentially equivalent to controlling the flight path angle (cf., e. g., [22]). The autothrottle is designed as a proportional-integral controller that maintains airspeed. Vertical speed control is realized by means of a cascade consisting of a proportional controller for vertical acceleration and a proportional-integral controller for vertical speed. Further, proportional pitch rate feedback is used to augment short period damping.
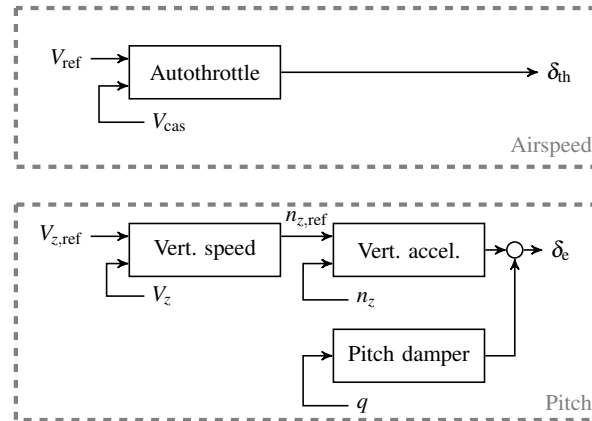
Fig. 5 Control architecture for longitudinal autopilot.

The lateral-directional autopilot, shown in Figure 6, follows a conventional architecture (e. g., [9]). Proportional-integral control of the bank angle is supplemented with proportional roll-rate feedback and the ailerons δ_a are used as the only effectors for roll control. Yaw control is realized by proportional-integral control of the sideslip angle, supplemented with yaw-rate feedback to increase dutch-roll damping. The effector for this control loop is the rudder δ_r. Choosing sideslip angle and

bank angle as the controlled variables is particularly suited for an automated approach: Wings-level can be assured and crosswind can effectively be accounted for by crabbing (cf., e. g., [22]).
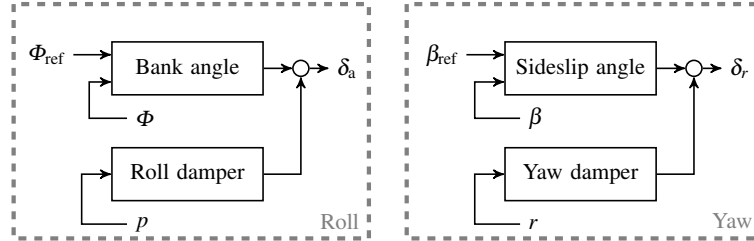

Fig. 6 Control architecture for lateral-directional autopilot.

All control loops were designed using classical loopshaping paradigms as briefly described in Section 3.1, see, e. g. [18, 19, 22] for their application in flight control.

4.2 Contact Model

Contact between the track-based landing system and the aircraft is modeled by means of one-sided spring-damper components at various points on the aircraft geometry. In particular, 5 points on the bottom of the center fuselage and central wing structure are used to model the touchdown on the contact rack or the ground, respectively. The altitude above the contact rack or ground is calculated for each point at each time instant in the simulation. When the distance becomes negative, contact is established and a reactive force is applied. This approach is equivalent to a simple penalty method (e. g. [23]). Coulomb friction is also added.

5 Simulation Results

Parameter values for the ground system model, provided in Table 1, are selected to perform a conceptual study. The controller gains are selected as detailed in Section 3.2, based solely on these model parameters. Table 2 further lists selected and resulting parameters for the control logic described in Section 3.3. Digital implementation of all control loops is performed with a sample rate of 100 Hz. The aircraft position and ground speed are assumed to be available with a sample rate of 10 Hz, with no additional delay. Kalman filters are used to upsample these measurements to 100 Hz as described in Section 3.4.

Figure 7 shows the simulation of a representative landing maneuver with a glide slope of $10°$. The aircraft approaches with a ground speed of about 12 m/s, starting

Table 1 Parameters for the model of the landing system.

Description	Variable	Value
Mass of complete landing system	m_x	$100\,\mathrm{kg}$
Mass of second trolley and contact rack	m_y	$30\,\mathrm{kg}$
Inertia of rotatable contact rack	J_Ψ	$1\,\mathrm{kg\,m^2}$
Damping coefficient for generalized coordinate x	d_x	$40\,\frac{\mathrm{Ns}}{\mathrm{m}}$
Damping coefficient for generalized coordinate y	d_y	$10\,\frac{\mathrm{Ns}}{\mathrm{m}}$
Damping coefficient for generalized coordinate Ψ	d_ψ	$1\,\frac{\mathrm{Ns}}{\mathrm{m}}$

**Table 2** Parameters for the control logic.

Description	Variable	Value
Velocity offset	V_{offset}	$0.5\,\mathrm{m/s}$
Position offset	x_{offset}	$3.0\,\mathrm{m}$
Switching distance	$x_{\mathrm{switch,pos}}$	$0.0\,\mathrm{m}$
Maximum force	$F_{x,\mathrm{max}}$	$1000\,\mathrm{N}$
Maximum force	$F_{y,\mathrm{max}}$	$250\,\mathrm{N}$
Maximum force	$M_{\Psi,\mathrm{max}}$	$10\,\mathrm{Nm}$
Resulting maximum acceleration in x direction	a_{max}	$8.3\,\mathrm{m/s^2}$
Resulting nominal activation distance	$x_{\mathrm{activation}}$	$10.2\;\mathrm{m}$

with a deviation of 1 m from the center line. Moderate crosswind and wind shear from 5–3 m/s with a relative angle of $-80°$ with respect to the track direction is considered. Further, mild turbulence with an intensity of 1 m/s is present during the approach.

The x-velocity and y-position control loop are activated first, at time $t \approx 4.2$ s. As a result, the first trolley starts to accelerate in x-direction up to the desired relative velocity of 0.5 m/s. Meanwhile, the second trolley acquires the y-position and the contact rack is aligned with the aircraft's heading angle. Once the aircraft is directly above the landing system ($t \approx 7$ s), the x-position control loop is activated. Shortly after, all degrees of freedom are successfully synchronized. The aircraft touches down on the landing system at $t \approx 9.6$ s and subsequently the trolley is decelerated to standstill. During this deceleration, small sliding motions of the aircraft in y-direction and in the heading angle are visible.

Details of the touchdown are shown in Figure 8. Immediately before the position control loop is activated, the relative x-velocity is close to the desired value of $V_{\mathrm{offset}} = 0.5$ m/s. The x-position error overshoot remains below 0.1 m and the error at touchdown is approximately 0.01 m. The error in y-direction is less than 0.05 m throughout the considered time range. The heading angle error at touchdown is less than 0.1 °. The sliding motion after touchdown, however, is relatively large. The angular velocity at impact is also significantly larger than the translational velocities, which hints at possible inaccuracies related to the rather crude contact model.

Given that the control system parameters are chosen solely based on the model parameters, the question of sensitivity of the proposed control system to parame-
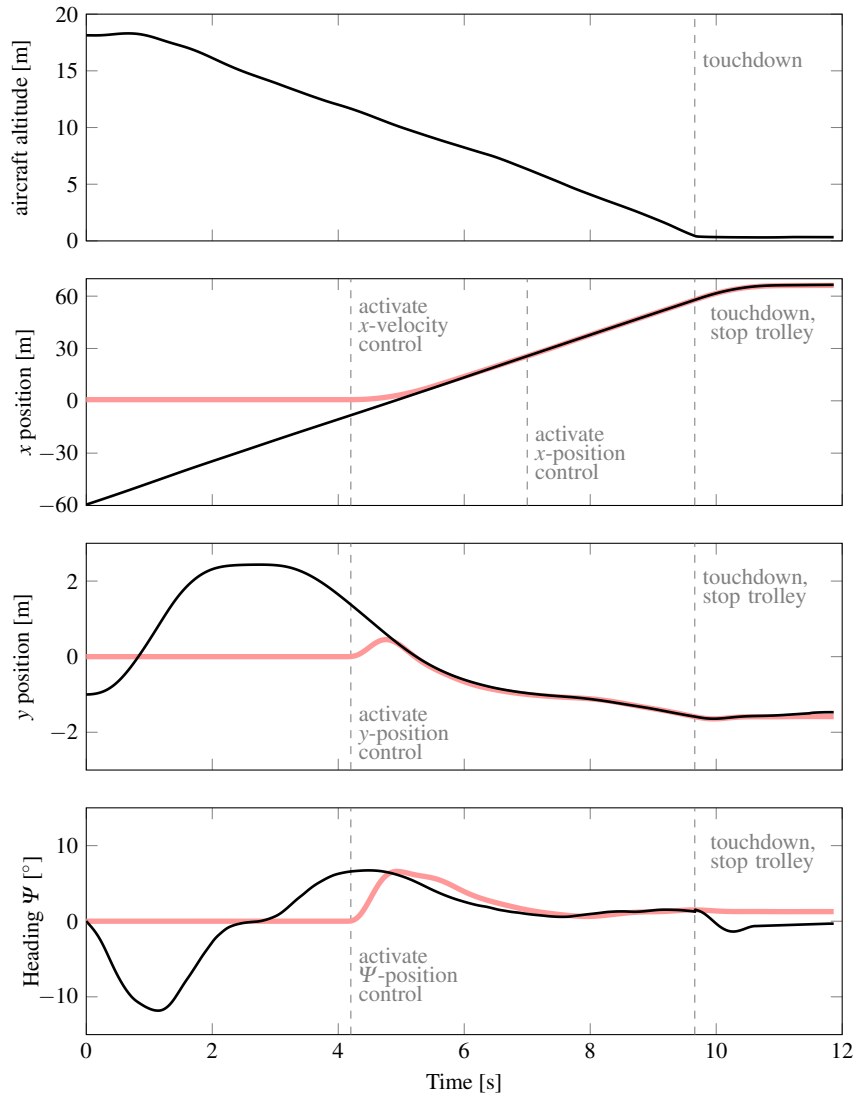
Fig. 7 Position of aircraft (———) and landing system (———) during approach.

ter uncertainty arises. To explore the sensitivity, the simulation presented above is repeated with the exact same control system, but perturbed model parameters in a Monte Carlo campaign with 1000 evaluations. The following uncertainty set is evaluated. The two generalized masses m_x and m_y are varied by $\pm 20\%$, as these parameters are easy to accurately obtain on any real system. All other parameters, i.e., the inertia, the damping coefficients, and the actuator time constants are varied
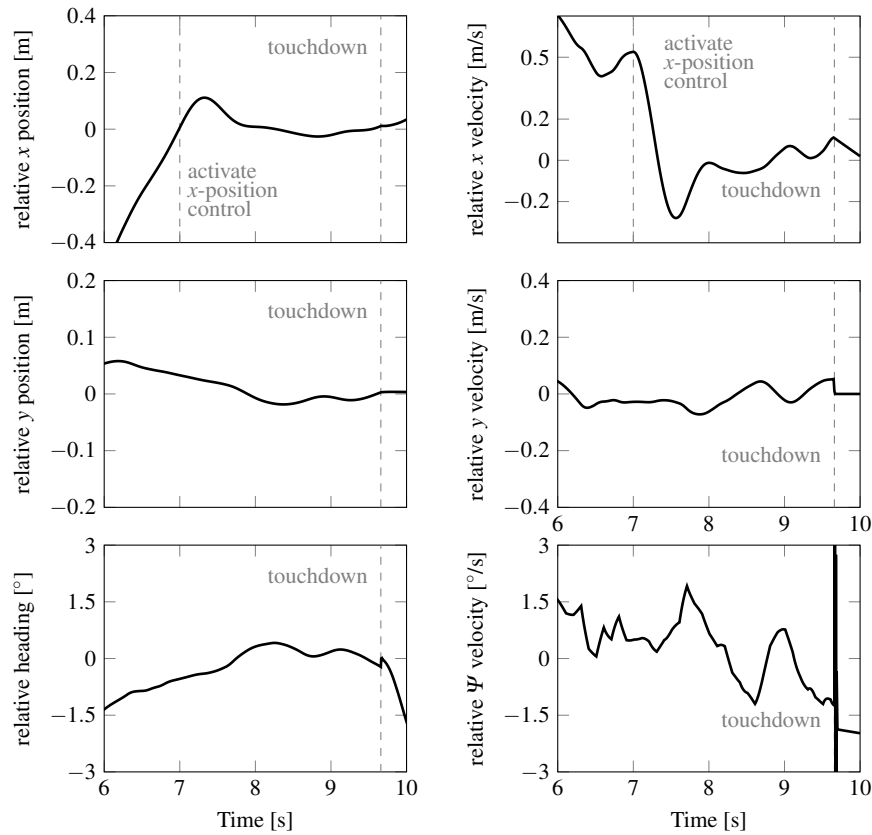
Fig. 8 Relative position and velocity around touchdown.

by ±50%. For all variations, uniform distributions are assumed in order to assess a variety of different combinations.

Figure 9 shows the resultant probability of the errors in all three degrees of freedom at touchdown. Note that the first 1% is enlarged to enhance legibility. The x-position error is on the order of 0.00–0.03 m in the vast majority of cases. The enlarged sub-one-percent scale shows that the largest outlier is at −0.4 m. A closer assessment of this simulation shows that it indeed corresponds to an extreme case of the considered parameter set. For the x-direction, the generalized mass was perturbed by almost −20%, the damping was perturbed by over −40% and the time constant of the actuator was perturbed by −45%. This explains some overshoot, in the position acquisition phase, which then causes the relatively large position error at touchdown. In the y-direction, the position error is much smaller and less than 0.01 m for almost all evaluated cases and the error in the heading angle Ψ is clearly below 1° for all considered cases. All three probabilities are mildly skewed. For both the y-position and the heading angle, this could be attributed to the presence

of crosswind. The skewness in the relative *x*-position might be a consequence of the false calculation of the activation distance due to the unknown mass, which could have more impact on the overall performance than the controller parameters. Still, it has to be concluded that the proposed control system handles the considered large parameter uncertainties extremely well. Overall, a worst-case accuracy of $-0.4\,\mathrm{m}$ to $+0.1\,\mathrm{m}$ in *x*-direction, $-0.03\,\mathrm{m}$ to $+0.02\,\mathrm{m}$ in *y*-direction, and $-0.8°$ to $0°$ in heading is achieved.
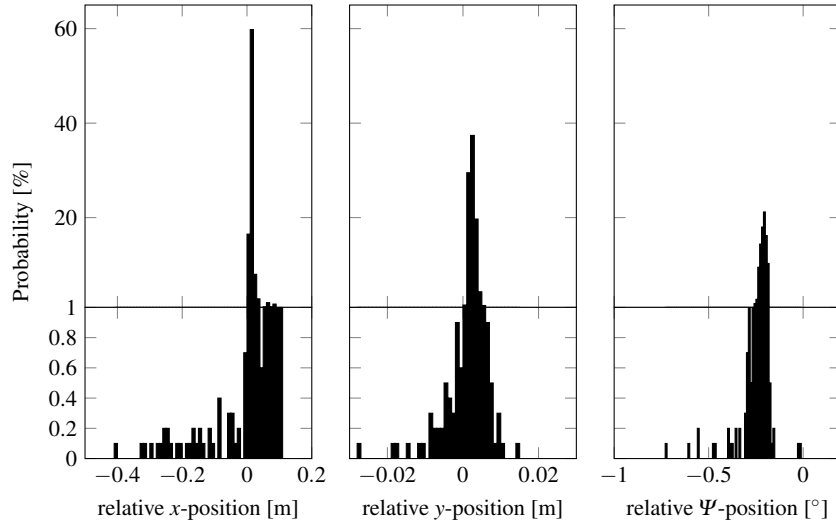

Fig. 9 Error at touchdown in Monte-Carlo simulation campaign with 1000 trials.

6 Conclusions and Outlook

The proposed control solution depends in closed form on the model parameters and is hence very easy to apply. For the considered simple model, it results in high-precision synchronization, even in the presence of disturbances and severe model parameter uncertainty. For actual application, additional delays and phase loss due to higher-order actuator or sensor dynamics are likely. These effects could be addressed through lead compensation in the most inner control loops such that the compensated dynamics again resemble the simplified model. In this case, the analytical controller parameters can be used as plausible initial values for controller tuning.

Besides providing a solution to the control problem, the proposed parameterization is also useful to derive a priori requirements for the development of a landing system. As the overall closed-loop bandwidth is known in terms of few model pa-

rameters, achievable performance can be assessed early in the design process. The simulation environment further allows quick evaluation of different approach scenarios, e.g., with different speed and glide slope. Further studies in this direction and also with a focus on the effect of time delay should be performed.

The simulation is set up such that it already has real-time capabilities. That is, it is possible to perform virtual flight testing with a UAV pilot in the loop. The pilot can control the aircraft through the autopilot system (i.e., control control sink rate and bank angle) or take conventional control of the flaps. Such virtual flight tests will be performed in the future to study possible interaction between active control of both aircraft and ground system. The initial simulation results also showed that a more accurate contact model should be incorporated. In particular, the geometry of the contact rack and the geometry of the aircraft need to be accurately modeled to evaluate potential threads of collision prior to touchdown.

References

1. Åström K, Hägglund T (2006) Advanced PID Control. The Instrumentation, Systems and Automation Society
2. Binnebesel, J (2008) Bodengebundene Vorrichtung für den Start-, Lande- und Rollvorgang von Flugzeugen. Patent DE 10 2008 023 698 B4
3. Brockhaus R, Alles W, Luckner R (2013) Flugregelung. Springer, Berlin
4. Cook M (2012) Flight Dynamics Principles. Butterworth-Heinemann
5. Decker BL (1984) World Geodetic System 1984. In: 4th International Geodetic Symposium on Satellite Positioning
6. Department of Defense (1997) Flying Qualities of Piloted Aircraft, MIL-HDBK-1797
7. Doyle J, Francis B, Tannenbaum A (1990) Feedback Control Theory. Macmillan Publishing Co.
8. European Aviation Safety Agency (2012) Certification Specifications and Acceptable Means of Compliance for Large Aeroplanes, CS-25, Amendment 12
9. Etkin B, Reid LD (1996) Dynamics of Flight: Stability and Control. John Wiley & Sons, New York
10. Horowitz, IM (1963) Synthesis of Feedback Systems. Academic Press
11. Jategaonkar R (2006) Flight vehicle system identification: a time-domain methodology. American Institute of Aeronautics and Astronautics, Inc.
12. Kreitz T, Bornholdt R, Krings M, Henning K, Thielecke F (2015) Simulation-Driven Methodology for the Requirements Verification and Safety Assessment of Innovative Flight Control Systems. In: SAE 2015 AeroTech Congress & Exhibition
13. McGeer BT, et al. (2001) Method for Retrieving a Fixed-Wing Aircraft Without a Runway. Patent US 6,264,140 B1
14. McRuer D, Ashkenas I, Graham D (1973) Aircraft Dynamics and Automatic Control. Princeton University Press, Princeton
15. Ohnishi K, Shibata M, Toshiyuki M (1996) Motion Control for Advanced Mechatronics. IEEE/ASME Transactions on Mechatronics 1(1):56–67
16. Rohacs D, Rohacs J (2016) Magnetic levitation assisted aircraft take-off and landing (feasibility study – GABRIEL concept). Progress in Aerospace Sciences 85:33-50

17. Rohacs D, Voskuijl M, Siepenkötter N (2014) Evaluation of Landing Characteristics Achieved by Simulations and Flight Tests on a Small-scaled Model Related to Magnetically Levitated Advanced Take-Off and Landing Operations. In: 29th Congress of the International Council of the Aeronautical Sciences
18. Schmidt, D (2012) Modern Flight Dynamics. McGraw-Hill
19. Sedlmair N, Theis J, Thielecke F (2019) Design and Experimental Validation of UAV Control Laws – 3D Spline-Path-Following and Easy-Handling Remote Control. 5th CEAS Conference on Guidance, Navigation & Control
20. Skogestad S, Postlethwaite I (2005) Multivariable Feedback Control. Prentice Hall
21. Steele DW (2008) Robotically Assisted Launch/Capture Platform for an Unmanned Air Vehicle. Patent US 7,410,125 B2
22. Theis J, Ossmann D, Thielecke F, Pfifer H (2018) Robust Autopilot Design for Landing a Large Civil Aircraft in Crosswind. Control Engineering Practice 76:54–64
23. Wriggers P (2006) Computational Contact Mechanics. Springer, Berlin
24. Wu P, Voskuijl M, van Tooren M (2014) Take-off and Landing Using Ground Based Power – Landing Simulations Using Multibody Dynamics. In: 52nd Aerospace Sciences Meeting